ACS APPLIED MATERIALS & INTERFACES

Research Article

www.acsami.org

Composites with Macroporous Poly(vinyl alcohol) Cryogels with Attached Activated Carbon Microparticles with Controlled Accessibility of a Surface

Yishan Zheng,[†] Vladimir M. Gun'ko,*[,†,‡] Carol A. Howell,[†] Susan R. Sandeman,[†] Gary J. Phillips,[†] Oleksandr P. Kozynchenko,[§] Stephen R. Tennison,[§] Alexander E. Ivanov,[∥] and Sergey V. Mikhalovsky[†,⊥]

[†]School of Pharmacy & Biomolecular Sciences, University of Brighton, Brighton BN2 4GJ, U.K.

[‡]Chuiko Institute of Surface Chemistry, 17 General Naumov Street, Kiev 03164, Ukraine

[§]MAST Carbon International Ltd., Jays Close, Viables, Basingstoke, Hants, RG22 4BA, U.K.

[∥]Protista Biotechnology AB, Kvarngatan 2, SE-26734, Bjuv, Sweden

[⊥]School of Engineering, Nazarbayev University, Kabanbay Batyr Avenue, Astana 010000, Kazakhstan

Supporting Information

ABSTRACT: A set of glutaraldehyde (GA) cross-linked poly(vinyl alcohol)/activated carbon (PVA/GA/AC) composites prepared in the form of monolithic rods using a cryogelation technique and studied using adsorption, mercury porosimetry, scanning electron microscopy (SEM), and quantum chemistry methods display porosity similar to that of PVA/GA cryogel at a high GA content (content ratio GA/AC = 1 and GA/PVA = 0.2). GA cross-linked PVA multilayer coverage is an effective barrier for adsorption on AC particles. Variations in surface chemistry (AC initial and oxidized in air at 300 °C for 12 h) and content (14−62.5%w/w) of ACs in PVA/GA/AC composites relatively weakly affect their textural characteristics at a high GA content (specific surface area S_{BET} < 120 m^2/g, pore volume V_p < 0.35 cm^3/g). However, PVA/GA/AC composite rods formed with a lower concentration of GA (content ratio GA/AC = 1/6 and GA/PVA = 1/10) have significantly greater S_{BET} (~500 m^2/g) and V_p (>0.55 cm^3/g) values because of improved accessibility of the AC surface. This provides better adsorption of methylene blue as a probe compound.

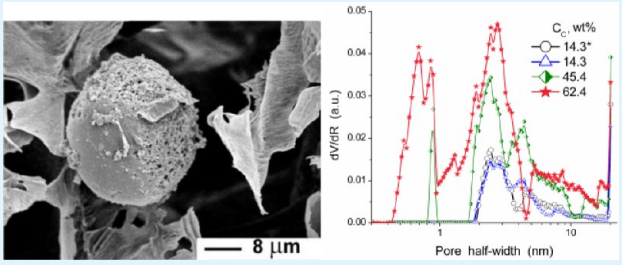

KEYWORDS: *activated carbon, glutaraldehyde cross-linked poly(vinyl alcohol), PVA/AC composites, textural characteristics, adsorption*

INTRODUCTION

Activated carbons (ACs) are effectively used not only in drinking water purification and various industrial applications but also in hemoperfusion- and hemofiltration-based therapies.[1] Recent technological advances[2,3] have allowed the production of ACs in both granular and monolithic forms that can be used for direct contact with blood without the need for an additional biocompatible coating.[4−7] The adsorption kinetics displayed by smaller AC microparticles (~1−50 μm) interacting with both low- (~10−100 atoms in molecules) and high-molecular (e.g., proteins, lipoproteins) compounds is more effective than that provided by larger AC granules or monoliths. This is due to the difference in the surface area accessibility and working layer thickness of smaller and larger AC particles. However, when using materials composed of microsized particles in a blood perfusion application, there is a problem related to microparticle retention within the device and pressure drop complications across the system. The application of ACs in different industrial and analytical adsorption devices can be accompanied by similar problems. To overcome these problems and prevent the loss of microsized AC particles, they can be attached by polymeric brushes to, or incorporated within, the walls of macroporous polymer hydrogels (cryogels). To combine the adsorptive potential of ACs with the low flow resistance of macroporous cryogel matrices, composites with ACs and polymeric hydrogels can be synthesized using a cryotropic gelation technique.[8−13] Investigations of materials formed by aggregation of poly(*N*-isopropylacrylamide-co-allylamine) nano-/microbeads and AC suggested the possibility of preparing elastic and spongy-like AC/polymer composites.[14] Various types of monolithic porous polymer structures (MPPS), produced by cryotropic gelation of water-soluble polymers, were developed by Protista (Sweden, www.protista.se). The structural and adsorption characteristics of AC/poly(vinyl alcohol) (PVA) composites have not previously been described in detail in contrast to carbon nanotube

Received: August 6, 2012
Accepted: October 22, 2012
Published: October 22, 2012

Table 1. Structural Characteristics of Carbons and PVA/GA and PVA/GA/AC Samples with the SCV/SCR-Model (MND)* and with the SC-Model (NLDFT)[a]

sample	content ratio PVA/GA/AC	S_{BET} (m^2/g)	S_{nano}* (m^2/g)	S_{meso}* (m^2/g)	S_{macro}* (m^2/g)	V_p (cm^3/g)	V_{nano}* (cm^3/g)	V_{meso}* (cm^3/g)	V_{macro}* (cm^3/g)	S_{NLDFT} (m^2/g)	Δw_{NLDFT}	c_{slit}*	c_{cyl}*	c_{void}*
AC1	0/0/1	724	448	266	11	0.955	0.147	0.578	0.230	675	0.073	0.648	0.255	0.097
AC2	0/0/1	842	511	305	27	1.020	0.102	0.328	0.590	786	0.072	0.680	0.252	0.068
AC3	0/0/1	1618	1146	469	4	1.332	0.455	0.773	0.104	1909	−0.180	0.658	0.291	0.051
AC4	0/0/1	1321	983	314	24	2.095	0.427	0.456	1.212	1784	−0.350	0.671	0.294	0.034
AC5	0/0/1	979	433	529	18	1.333	0.161	0.845	0.327	1032	−0.054	0.646	0.295	0.059
PVA/GA	5/1/0	78	1	76	2	0.212	0.0	0.162	0.050	84	−0.063	0.684	0.124	0.192
PVA/GA/AC1	5/1/1	69	0	64	5	0.210	0.0	0.107	0.103	70	−0.017	0.112	0.715	0.173
PVA/GA/AC2	5/1/1	62	0	57	4	0.191	0.0	0.096	0.095	62	−0.006	0.387	0.440	0.174
PVA/GA/AC3	5/0.5/3	499	264	233	2	0.634	0.076	0.497	0.061	467	0.042	0.328	0.575	0.097
PVA/GA/AC4	5/0.5/3	488	323	160	5	0.549	0.108	0.314	0.127	567	−0.162	0.057	0.892	0.051
PVA/GA/AC5	5/1/10	119	47	69	3	0.343	0.015	0.207	0.120	120	−0.008	0.115	0.872	0.013

[a]Note. Contribution of nanopores (S_{nano}, V_{nano}) at radius (half-width for slit-shaped pores) $R < 1$ nm, mesopores (S_{meso}, V_{meso}) at $1 < R < 25$ nm, and macropores (S_{macro}, V_{macro}) at $R > 25$ nm; Δw is the relative deviation of the pore shape from the SC-model; c_{slit}, c_{cyl}, and c_{void} are the weight coefficients of slit and cylindrical pores and voids between spherical particles, respectively, calculated using the MND method with the self-consistent regularization procedure (SCV/SCR model).

(CNT)/PVA composites,[15−19] PVA/carbon electrodes,[20] and some other PVA-based composites.[21−26] The accessibility of the surface of CNT incorporated in composites[15−19] or the carbon component in PVA/carbon electrodes[20] has not been analyzed. Nanostructured organic−inorganic composites (mixed at molecular or near molecular level) are very different from the conventional composites, with incorporation of a variety of nano-, micro-, or macroparticles into the polymer matrices. Significant efforts have been focused on the development of methods to prepare novel hybrids with desired properties and functions, such as the sol−gel method, intercalation, and other techniques.[21−26] PVA has been used for preparation of cryogels[5−11] and the composites including a variety of fillers.[21−26] Activated carbons or other carbon forms (e.g., CNT) as fillers in composites can be used as effective adsorbents in a range of medical, industrial, and environmental protection applications.[1−7,27−30] ACs with a significant textural porosity caused by the presence of voids between nano-/mesoporous nanoparticles packed within microsized granules can be effective adsorbents for both low- and high-molecular compounds.[31−37] The AC activation (burn-off) degree can also strongly influence the textural and framework-confined porosities in addition to altering the amounts of oxygen-containing surface functionalities affecting the adsorption properties of the materials especially in aqueous media.[31−37] Clearly, in composites with polymers and ACs, retaining these textural features of carbons and good accessibility of the AC surface for target adsorbates is of importance.

Polymer hydrogels are used in numerous biomedical and pharmaceutical applications because they can be produced from precursors possessing appropriate biocompatibility profiles and mechanical properties approaching those of natural tissues.[38−41] Of special interest for medical applications are hydrophilic cryogels with a pore size $d > 1$ μm and great macroporosity (10−15 cm^3/g or higher) and high interconnectivity allowing the flow of cellular or acellular bodily fluids through the matrix. Notice that this macroporosity cannot be determined from the nitrogen adsorption isotherms, but it can be estimated from the amounts of water in superhydrated cryogels or microscopic images.

Cross-linking of polymer−polymer or polymer−AC nano-/microparticles (with possible participation in the reactions of surface O-containing functionalities of ACs) is an important aspect in preparation of the AC/PVA composites because their characteristics can strongly depend on the cross-linking degree. The interfacial behavior of PVA plays an important role in the preparation of membranes,[42] composites with graphene,[43] CeF_3[44] and Ag[45,46] nanoparticles, a barrier layer of a nanofiltration polysulfone membrane,[28,47] and other systems. However, the cross-linked PVA can block pores of AC in PVA/AC composites which is a rather negative effect. From our experience and analysis of the literature,[48−50] it is expected that the regularities in the textural characteristics of PVA/AC composites can be characteristic for AC-filled cryogels prepared with other polymers or proteins cross-linked by low-molecular compounds.

The aim of this work was to prepare glutaraldehyde cross-linked PVA cryogel/AC composites with controlled textural characteristics studied using adsorption, mercury porosimetry, microscopy, and quantum chemistry methods. This study provides an understanding of the molecular interactions between carbon microparticles (initial and additionally oxidized) and polymers and explains the textural features of the composites and the interfacial behavior of PVA/GA. Maximum accessibility for adsorbates of a surface of AC microparticles incorporated into the PVA cryogels is desirable for practical applications of the composites; therefore, preparation of such materials was one of the aims of the work.

EXPERIMENTAL SECTION

Materials Synthesis. Poly(vinyl) alcohol, PVA (Mowiol 8−88, Sigma-Aldrich 81383), with molecular weight of 67 kDa and 86.7−88.7 mol % hydrolysis was used to prepare the cross-linked PVA cryogel. Glutaraldehyde (GA, $HC(O)(CH_2)_3C(O)H$, EM grade 25 wt %/v, Agar Scientific, R1012) was used as a cross-linker for the PVA cross-linking during cryogelation.[8−13] GA, dissolved in an aqueous medium and exposed to physiological pH for a relatively long period of time, tends to undergo self-polymerization.[51] The GA water-soluble oligomers thus produced include α,β-unsaturated formyl groups. These oligomers, in addition to the GA monomers, seem to play a significant role in the cross-linking.[51] The mechanism of cross-linking reaction between GA and PVA includes several stages resulting in the formation of such bonds as $(-C(H_2)-C(H)-O)_2CH(CH_2)_3C(H)-(O-C(H)-CH_2-)_2$ (i.e., four C−O−C bonds between a GA molecule and PVA) and other bonds with the participation of GA oligomers and polymers in the reactions with PVA.[51,52] Ethanolamine with the concentration of 0.3 M and adjusted pH 8.5 was used for blocking the possible free aldehyde groups after the PVA cryogelation.

dx.doi.org/10.1021/am301577c | ACS Appl. Mater. Interfaces 2012, 4, 5936−5944

Hydrochloric acid (5 M) was used to adjust the pH for all the solutions. Activated carbon (AC) microbeads (average particle size 20 μm, MAST Carbon International Ltd., UK)[53] were used for the composite synthesis. They were prepared from microspherical porous phenolic resin.[2,3] Carbon 1 (AC1) was the initial AC. Carbon 2 (AC2) was additionally oxidized in air in a shallow bed at 300 °C for 12 h to cover the surface with oxygen-containing groups, mainly carboxylic (~0.6 mmol/g) and phenol-type hydroxylic (0.6 mmol/g), as established by acid−base (Boehm) titration. These groups can form hydrogen bonds with PVA hydroxyls or participate in the cross-linking reactions with the GA monomers, oligomers, and polymers. In other words, in the PVA/AC composite not only cross-linking of PVA molecules via GA occurs but also PVA−GA−AC and AC−GA−AC bonds can form. This chemical aspect is of importance to understand textural features of PVA/GA/AC composites (Table 1 shows representative samples of different types).

GA cross-linked poly(vinyl alcohol) and AC-filled cross-linked PVA samples were prepared using a cryogelation technique.[8−13] In the case of the first series of samples, a 5% (wt/v) PVA solution was prepared by dissolving the polymer in water at elevated temperature. After adjusting the pH to 1.0−1.2 using 5 M HCl, the solution was cooled on ice for 30 min. Glutaraldehyde (1% final concentration) was added to the PVA solution as the cross-linking agent before the mixture was frozen at −18 °C for 18 h. In the case of PVA/GA/AC composite preparation, AC beads were suspended in water then added to 8% PVA solution to achieve a 5% PVA final concentration and 1% (wt/v) AC. After mixing the chilled PVA/AC mixture, GA with the final concentration of 1% w/v was added before the mixture was pipetted into the syringes and frozen at −18 °C for 18 h. The monolithic cryogel rods were defrosted at room temperature and washed with water before the 0.3 M (pH 8.5) aqueous ethanolamine solution was used to block the possible remaining aldehyde groups at room temperature for 2 h. Additionally, a mechanical AC/PVA/GA cryogel mixture was also prepared by shaking the shredded dry PVA/GA cryogel with AC beads before reswelling the mixture in 1% GA solution. The cryogel rods and mechanical mixture were frozen at −18 °C for 30 min before loading into the freeze-dryer overnight.

To analyze the effect of the surface chemistry of ACs, PVA/AC composites were made using the initial ACs and ACs oxidized in air. It should be noted that the oxidation in air at 300 °C for 12 h or oxidation of AC by concentrated acid solution have a relatively weak effect on the structural characteristics of carbons alone according to the small-angle X-ray scattering data and the pore size distributions (PSDs) for similar AC materials.[54]

The freeze-dried samples were used for SEM imaging. The samples used for low-temperature nitrogen adsorption analysis and mercury porosimetry were degassed for 24 h at 40, 80, and 100 °C in a vacuum oven after freeze-drying. An ambient temperature (40 °C) of degassing can result in residual water remaining in the pores of ACs. This water can affect the nitrogen adsorption, but it is unlikely to affect the adsorption properties of materials used in aqueous media for, e.g., blood purification, protein adsorption, etc. Therefore, some samples were degassed at different temperatures to analyze the effect of residual water.

Materials Characterization. *Nitrogen Adsorption.* Nitrogen adsorption−desorption isotherms were recorded at 77.4 K using an Autosorb (Quantachome Instruments, USA) adsorption analyzer. The pore size distributions (PSDs) were calculated using two models of pore mixtures of (i) slit-shaped and cylindrical pores for carbons (SC-model) with the nonlocal density functional theory (NLDFT) method[54] (Quantachrome software) and (ii) slit-shaped (carbon) and cylindrical (carbon or polymer) pores and voids between spherical particles (carbon) using the modified Nguyen-Do (MND) method (SCV-model) with a self-consistent regularization (SCR) procedure.[55−58] The differential PSDs $f(R) \sim dV/dR$ ($\int f(R)dR \sim V_p$, where R is the pore radius or half-width) were converted into incremental PSDs ($\sum\Phi(R_i) \sim V_p$) for a better view of the PSDs over total pore range. The errors of the SC pore model were calculated as $\Delta w = S_{BET}/S_{NLDFT} - 1$ (Table 1).[58]

Mercury Porosimetry. This technique with a PoreMaster (Quantachome Instruments, USA) was used to determine the macropore size distributions of samples (differential PSD $f(d) \sim dV/dd$ or for a better view of contribution of larger pores as $-dV/d(\log d)$ where d is the pore diameter).

SEM. For scanning electron microscopy (SEM) analysis, the freeze-dried gel samples were sputter coated with a 50 nm thick layer of gold or without coating and examined using scanning electron microscopy (SEM JSM-6310, Japan Electron Optics Ltd., and Carl Zeiss SMT Ltd., UK). The results based on the nitrogen adsorption are in agreement with SEM images and mercury porosimetry.

Quantum Chemical Calculations. Quantum chemical calculations of interactions of PVA fragments with different carbon structures were carried out using Gaussian 03[59] and GAMESS (versions WinGAMESS 10.2[60] and Firefly 7.1G[61]) packages with ab initio and DFT (B3LYP) methods with consideration of solvation effects (IEFPCM method, B3LYP/6-31G(d,p) basis set) (up to 185 atoms) and the PM6 method (MOPAC 2009 and 2012 with the MOZYME algorithm)[62] (up to ~7000 atoms). The initial structure of large models was optimized using the CharMM force field (Vega ZZ 2.4[63] with NAMD 2.7b3[64]). Structures were visualized using Vega ZZ, Jmol,[65] or ChemCraft[66] programs.

RESULTS AND DISCUSSION

Prior to their incorporation into PVA/GA cryogels, the microspherical AC samples (beads of 10−30 μm in diameter) were shown to contain different internal porosity (V_p) and specific surface area (S_{BET}) with significant contributions from nanopores (at pore radius or half-width $R < 1$ nm), mesopores ($1 < R < 25$ nm), and macropores ($R > 25$ nm) (Table 1 and Figure 1 show representative samples of ACs, PVA/GA, and PVA/GA/AC). The ACs used are characterized by a broad pore size distribution (PSD) of a complex shape as seen in Figure 1.

Despite the dependence of the PSD shape on the pore models used, the general features of the two types of PSDs of nanopores and mesopores are similar for the NLDFT (SC-model) and MND (SCV/SCR-model) methods. The MND method with the SCV/SCR-model was applied to a larger pore range ($0.35 < R < 100$ nm) including macropores than NLDFT ($R < 20$ nm, SC-model) applied only to nano- and mesopores. Carbon nanoparticles, which are strongly aggregated in microparticles, and voids between them are of complex shapes (Figure 2).

However, motifs of slit-shaped (in nanoparticles) and cylindrical pores and voids between nanoparticles can be found in the images.[33−35,53] According to calculations with the SCV/SCR-model, slit-shaped pores provide the main contribution (~2/3) to the carbon porosity (Table 1, c_{slit}), and the contribution of cylindrical pores ($c_{cyl} \approx 0.25-0.30$) is larger than that of voids between spherical particles ($c_{void} < 0.1$). The small c_{void} values are in agreement with small Δw_{NLDFT} values (Table 1), showing a small deviation of the pore shape from the SC-model (NLDFT) for several ACs. For AC samples with great S_{BET} values and large macroporosity (AC3 and AC4, Table 1), the Δw_{NLDFT} value increases due to restriction of the range of NLDFT PSD calculated at $R < 20$ nm. The values of $\Delta w_{SCV/SCR} = 0.042$ (AC3) and 0.125 (AC4) are smaller because of consideration of larger pore sizes in the calculations with a more complex SCV model and the SCR procedure which are absent in the Quantachrome software used.

The mercury porosimetry data (Figure 3) show a significant contribution of narrow macropores in the same range of sizes as the MND PSDs show (Figure 1). These macropores can be attributed to voids between nanoparticles in microparticles

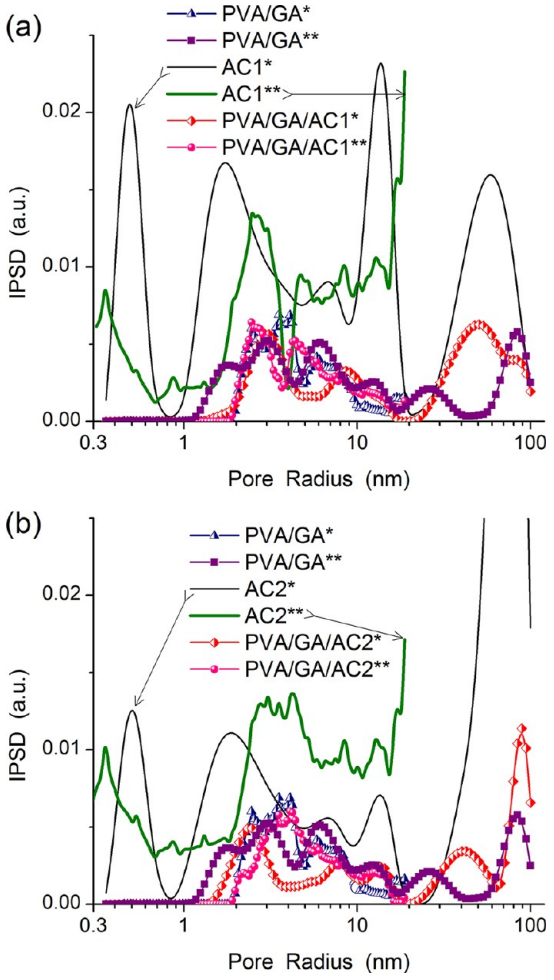

Figure 1. Incremental PSDs with the model of a mixture of (*) slit-shaped (carbon nanoparticles) and cylindrical (carbon or polymer) pores and voids between spherical particles (carbon) (MND) and (**) slit-shaped and cylindrical pores for carbons (NLDFT) for PVA/GA and (a) AC1 and PVA/GA/AC1; (b) AC2 and PVA/GA/AC2.

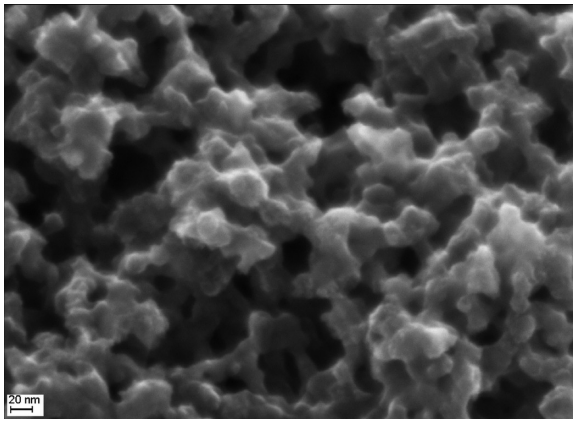

Figure 2. SEM image of the inner texture of AC composed of nanoparticles (scale bar 20 nm).

(Figure 2). The main peak of the carbon PSDs at $d \sim 0.1$ μm (Figure 3) corresponds to the macropore peak obtained from the nitrogen adsorption with the SCV/SCR pore model (Figure 1). Consequently, one can assume that AC particles maintain their integrity throughout measurements at high Hg pressures. However, during similar measurements of PVA/GA

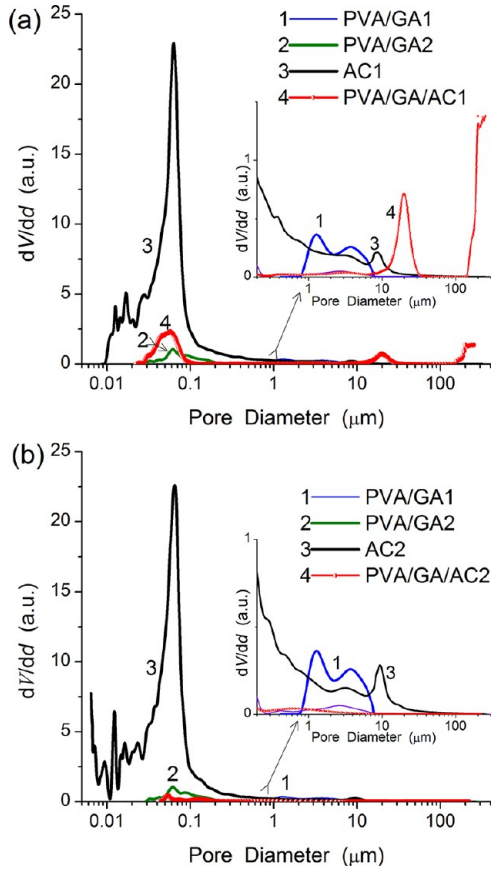

Figure 3. Differential PSD (dV/dd) based on the mercury porosimetry data for two PVA/GA samples and (a) AC1 and PVA/GA/AC1; (b) AC2 and PVA/GA/AC2; insets show a portion of the PSDs at $d > 0.2$ μm.

and PVA/GA/AC composites, a significant loss of the macroporosity is seen (by an order of magnitude, compare the PSD intensity for AC and PVA/GA, PVA/GA/AC in Figure 3) due to the high Hg pressure (intrusion run) used and the softness of the polymeric materials.

Comparison of the PSDs based on Hg porosimetry and SEM image analysis of a PVA/GA sample (Figure 4) shows a clear shift of the porosimetry distribution function toward smaller pore sizes because of the mentioned compaction effect.

According to SCV/SCR calculations, the contribution of slit-shaped pores (Table 1, c_{slit}) decreases, but the contribution of cylindrical pores (c_{cyl}) and voids (c_{void}) increases in PVA/GA/AC composites in comparison with ACs alone. The broad PSDs that are important for the adsorption of both small and large molecules and thus for the practical application of ACs as medicinal adsorbents can be adversely affected by the interaction of the carbon microparticles with PVA (Figures 5 and 6).

During cryogel synthesis, GA can cause chain scission of PVA in addition to the cross-linking. This effect can be stronger during synthesis of the materials in aqueous media at $T > 0$ °C. In the case of cryogelation at −18 °C, the polymeric walls of macropores undergo high pressure from ice crystallites (volume of which is larger than liquid water) formed during cryogelation. Therefore, the inner porosity of the soft polymeric walls is low as $S_{BET} < 80$ m^2/g and $V_p \sim 0.2$ cm^3/g (Table 1, PVA/GA). If the degree of scission of PVA by GA is high, the

dx.doi.org/10.1021/am301577c | ACS Appl. Mater. Interfaces 2012, 4, 5936−5944

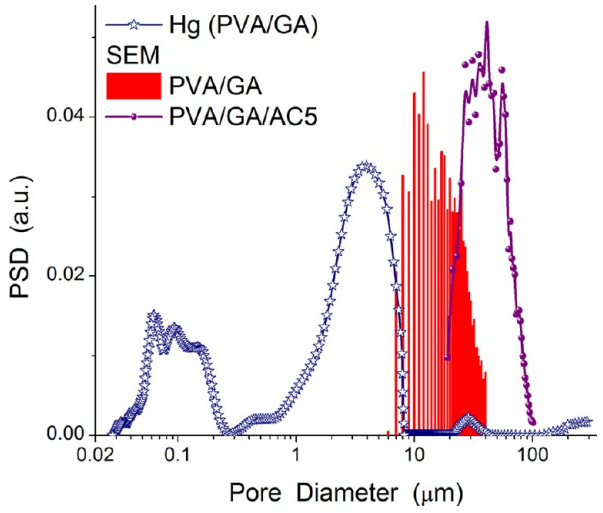

Figure 4. PSD based on the mercury (HG) porosimetry and SEM image analysis[67] for PVA/GA and PVA/GA/AC5.

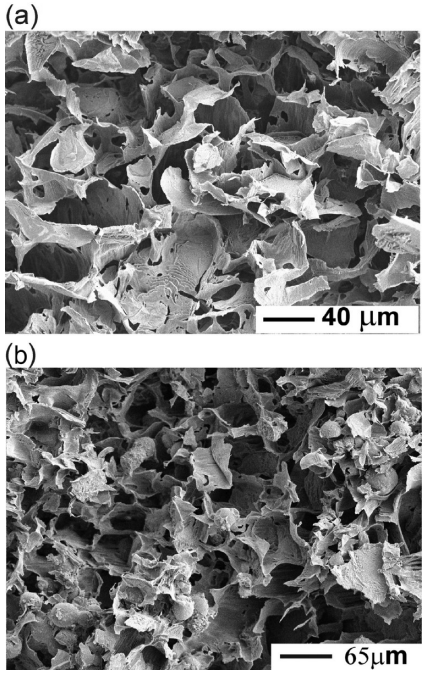

Figure 5. SEM images of the (a) freeze-dried PVA/GA cryogel and (b) PVA/GA/AC1 composite.

S_{BET} value could be as large as that observed for porous polymers (up to 1500 m^2/g).[57]

GA cross-linked PVA can cover the outer surface of AC beads by continuous or fragmentary films. In the first series of samples, PVA/GA totally blocks or fills the narrow pores (R < 1−2 nm) since linear polymers and GA (monomers, oligomers) can penetrate into narrow pores and be cross-linked there (AC surface hydroxyls can participate in cross-linking reactions with GA/PVA). This significantly reduces accessibility to mesopores at 1 < R < 25 nm. There is a shift of PSD of PVA/GA/AC in comparison with PVA/GA at R = 1−2 nm (NLDFT for all samples and MND for certain samples). This result can be explained by the strong interactions that exist between the PVA/GA and AC surface (Figure 6).

Mesopores at 1 < R < 10 nm give the main contribution to the porosity of PVA/GA/AC samples. However, the random

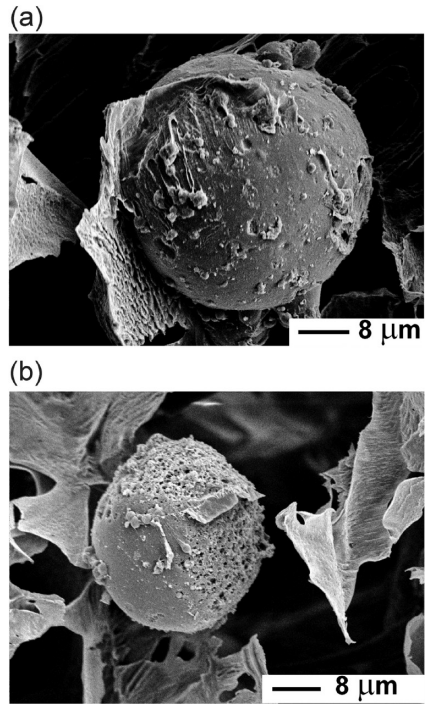

Figure 6. Scanning electron micrographs of PVA/GA/AC composites showing AC particles attached to freeze-dried cryogels with (a) AC1 and (b) AC2.

structure of PVA macropores and narrow pores in both AC particles and PVA/GA films do not allow us to give detailed analysis of the features of pores and their assignment to PVA/GA or AC. The SEM image (Figure 2) shows the inner texture of AC consisting of dense aggregates of nanoparticles (20−50 nm) with voids between them constituting transport of meso- and macropores. However, in the case of PVA/GA/AC composites (Figures 5 and 6), multilayer PVA/GA coverage can block this inner texture from adsorbates.

The pore wall thickness of the PVA/GA gel (~1−3 μm for dried samples) is smaller than the AC microparticle size (Figures 5 and 6). The pore walls with PVA/GA are soft and flexible. Therefore, during mercury porosimetry measurements at high pressures, the contribution of pores at 0.03 < d < 0.3 μm is larger for PVA/GA/AC1 than for GA/PVA alone (Figure 3a). This can be due to the pore contribution of AC in the composites (Figure 6).

Thus, synthesis of the PVA/GA cryogel in the presence of the carbon microparticles in the reaction medium results in a considerable diminution of the accessibility of AC surface and pores even for small nitrogen molecules. Notice that macropores visible in SEM images of AC particles (Figure 6) are not the main adsorption space for nitrogen (Figure 1), but Hg can completely fill them during the porosity measurements (Figures 3 and 4). Therefore, a mechanical mixture of ACs with PVA/GA cryogel in the cross-linker GA solution was prepared to attach AC microparticles to the PVA macropore walls. However, the flexibility of the PVA pore walls and the presence of GA monomers and oligomers as well as mobile PVA tails and trains cause too strong attachment of AC microparticles to the PVA structures by GA and blocking of AC pores by GA oligomers. A relatively low specific surface area of these samples (at maximal AC content C_{AC} = 62.5 wt %, S_{BET} = 119 m^2/g) can be considered as evidence of cross-linking of AC surface

dx.doi.org/10.1021/am301577c | ACS Appl. Mater. Interfaces 2012, 4, 5936−5944

hydroxyls with PVA by GA and AC pore filling by organics. Therefore, the AC surface blocking by PVA/GA is significant but incomplete in contrast to the first series of PVA/GA/AC samples (compare PSDs in Figures 1 and 7). It should be noted

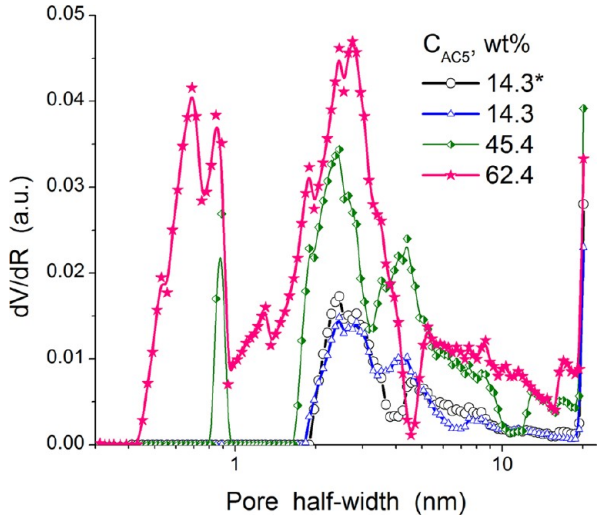

Figure 7. Influence of the concentration of AC5 in the PVA/GA/AC5 composite on the NLDFT PSD (*sample was heated at 80 °C, other samples were heated at 100 °C for 24 h prior to measurement).

that the specific surface of macropores of PVA/GA is about 1 m^2/g, i.e., ~1% of S_{BET}.[50] The major portion of the S_{BET} value is provided by the inner porosity of the walls of macropores. The V_p value of pores in these walls is ~0.2 cm^3/g, which is smaller than the macropore volume by 2 orders of magnitude.[50]

An increase in the AC5 content in the composite results in an increase in the contribution of narrow nanopores (Figure 7), and the accessible AC pore volume increases (compare the PSD intensity in Figures 1 and 7). On the basis of the results for two types of composites, one can assume that better results can be obtained at smaller C_{PVA} values in PVA/AC and smaller amounts of a cross-linker (GA) because both components can block/fill pores of AC particles. However, an increase in the AC content to 45.4−62.5 wt % leads to a decrease in the composite material elasticity. Notice that degassing of the composites at 80 or 100 °C gives very similar PSDs (Figure 7, sample at C_{AC5} = 14.3 wt %); i.e., samples have good thermal stability.

The AC surface includes different oxygen-containing functionalities (−COOH, ≡COH, ≡C−O−C≡, >C═O, ≡C−O−C═O),[27−37] which can strongly interact with PVA through hydrogen bonds (>O_{AC}···HO_{PVA} or ≡COH_{AC}···O-(H)C_{PVA}) and dispersion forces or be cross-linked (COH, COOH) by GA. To model these interactions, quantum chemical calculations of complexes of a PVA fragment (four units) with different AC functionalities (Tables S1 and S2 in the Supporting Information) were carried out with consideration for solvation effects using the IEFPCM method (B3LYP/6-31G(d,p) basis set) and the geometry optimization using the HF/6-31G(d,p) method for small models (PM6 method was used for large models, Figure 8).

Changes in the free energy (ΔG) upon PVA complex formation are in the range of −14 to −30 kJ/mol and −30 to −55 kJ/mol (per a bond or a hydrogen bond) for hydrophobic (without O-containing groups) and hydrophilic O-containing functionalities of the AC models, respectively (Table S1 in the Supporting Information). These values are close to that for

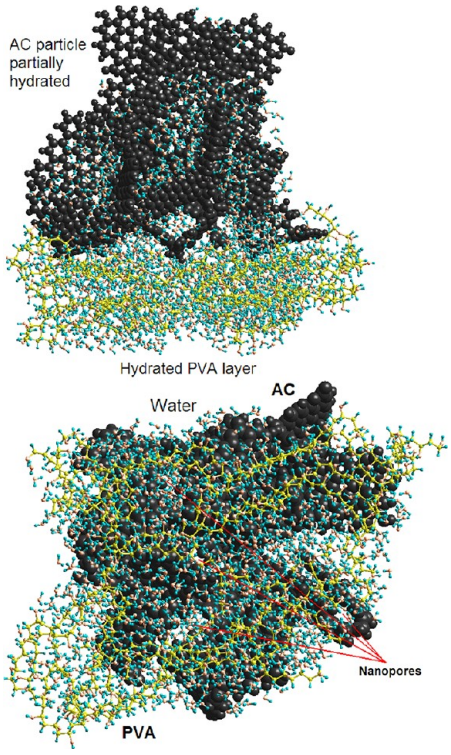

Figure 8. Interaction of GA cross-linked PVA (~2000 atoms) with AC (~1700 atoms) in the presence of water (~1100 molecules) (the geometry was optimized by PM6/MOZYME). Pictures show two sides of the same system.

complexes with water molecules and both PVA and AC. However, PVA having many contact points with the carbon surface can displace a portion of water molecules from both the pores and outer surface of AC particles (Figure 8). The initial 3D particle model (~1700 carbon atoms) of AC was developed with a number of 2D carbon sheet fragments on the basis of the Monte Carlo modeling of AC structure[68−70] and HRTEM images of ACs[71] similar to carbons used here. For initial optimization of the geometry of the built model, the molecular mechanics (MM) with the CharMM force field[63] was used. Then, the obtained geometry was reoptimized using the semiempirical PM6 quantum chemical method with the MOZIME algorithm (MOPAC 2009 program suit).[62] Then, water molecules (~1100H_2O) were added to this AC particle placed into the solvation box using the VEGA ZZ 2.4[63] program suit. A polymer shell fragment with GA (~5 wt %) cross-linked PVA (~2000 atoms) was built at the hydrated AC particle, and the geometry of the system was optimized using the CharMM force field and then reoptimized with the PM6/MOZIME method (Figure 8). The PVA/GA shell with two to three monolayers has mobile tails and trains that allow it to form relatively dense coverage of the hydrated AC particle from one side (Figure 8a). During the optimization of the geometry, the PVA/GA shell displaces a portion of water from one side of the AC particle surface in the contact zone (Figure 8). Calculations (with PM6) of the interaction energy (per water molecule or one PVA−AC bond) give $\Delta E \approx -10$ kJ/mol for PVA/GA−water interactions, −24 for PVA/GA−AC, −32 for AC−water, and −41 for PVA/GA−AC−water interactions. These values, which are in agreement with published results on interactions of AC with water,[31−37] show that the interactions between PVA and AC are weaker than that between AC and

dx.doi.org/10.1021/am301577c | ACS Appl. Mater. Interfaces 2012, 4, 5936−5944

water but stronger than that between PVA and water. Despite these values, PVA can displace water molecules because of kinetic/statistic effects since the number of intermolecular bonds between PVA and AC is much greater than the number of bonds between a water molecule and the AC surface. Thus, larger molecules displace smaller molecules from a surface which is a typical effect.[57]

To model the opposite effect with possible displacement of a small PVA fragment by water molecules from narrow pores (~0.7 nm in size), the pore size was fixed by the GA cross-linking of corners of two carbon sheets with several O-containing functionalities (Table S2 in the Supporting Information). The ΔG values (i.e., changes in the Gibbs free energy due to interactions of solvated components) for the PVA fragment (four units) and water complexes in this pore are similar (~ −30 kJ/mol calculated using IEFPCM/B3LYP/6-31G(d,p)). However, out of five water molecules placed in the pore around the PVA fragment, three escaped in contrast to the PVA fragment (Table S2 in the Supporting Information). Despite the positive ΔG value for this complex, the PVA fragment is not removed from the pore due to high energetic barrier of this motion. Additionally, PVA can form relatively tight complexes with the AC surface in the presence of water (Figure 8). Strong retention of PVA (tails and trains), as well as GA oligomers and polymers, within narrow pores (nanopores and mesopores) and at the outer surface (i.e., in macropores, Figure 6) of AC particles explains textural features of PVA/GA/AC composites with PVA/GA-blocked narrow pores of AC particles. Notice that PVA tails and trains have a high mobility in cryogels.[72] Consequently, to maintain the AC porosity, carbon particles should be attached to the surface of PVA/GA macropores after cryogelation, and the GA amounts used for cross-linking should below.

The oxidation of the carbon surface can be used to increase interactions of hydrophilic polymer to hydrophilic segments of the AC surface. Covalent bonds are possible (e.g., −C(O)OH of carbon + C(H)(OH)═ of polymer → −C(O)OC(H)═) but unlikely without coupling agents. If free aldehyde groups of cross-linked PVA/GA are blocked with ethylenediamine, there is a possibility to form a link to the surface COOH group via ion-pair formation. However, the chemical modification of ACs by oxidation in air does not practically affect the textural characteristics of the PVA/GA/AC composites because of the high amounts of PVA/GA forming multilayer coverage on the AC microparticles.

Calculations of changes in the free energy in the cross-linking reactions with consideration of the solvation effects using the IEFPCM/B3LYP/6-31G(d,p) method show that the reactions can more easily occur according to the mechanism described previously[51,52] with the participation of PVA (a four-unit fragment used) than the AC (modeled by a two-ring fragment). For instance, ΔG = −80.1 kJ/mol (cross-linking PVA−GA−PVA with the formation of four C−O−C bonds and elimination of two H_2O molecules), −7.6 kJ/mol (AC-(OH)−GA−(HO)AC), 4.3 kJ/mol (AC(COOH)−GA−(HOOC)AC), −41.4 kJ/mol (AC(COOH)−GA−PVA), and −12.9 kJ/mol (AC(OH)−GA−PVA). These differences in the ΔG values can be explained by a higher flexibility of the PVA chain in comparison with the O-containing functionalities attached to the aromatic structures in ACs. However, there is an additional aspect of the influence of these AC functionalities since the acidic groups (−COOH) can catalyze the oligomerization and polymerization of GA. These larger molecules can more effectively block the AC pores during the preparation of the mechanical mixture with GA-cross-linked PVA and ACs in the GA solution. Therefore, significant loss of the porosity and accessible AC surface is observed for these samples.

On the basis of the results obtained for composites prepared at relatively large amounts of GA, another series of composites was prepared using the same technique but with a decreased amount of GA and an increased content of AC. The reaction composition included 5 wt % PVA, 3 wt % AC, and 0.5 wt % GA; i.e., the ratio C_{GA}/C_{AC} was decreased by six times. Additionally, AC samples (Table 1, AC3 and AC4) used were with large S_{BET} values. The diminution of the GA content results in the formation of the composites PVA/GA/AC3 and PVA/GA/AC4 with much larger S_{BET} and V_p values than that of composites of the first series. The NLDFT PSDs demonstrate (Figure 9) that these composites are characterized

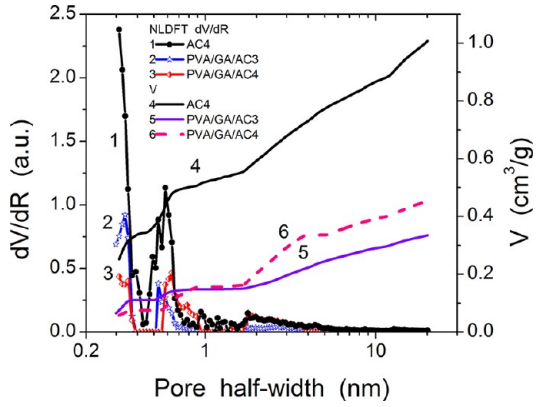

Figure 9. NLDFT PSD (SC model) for AC4 and PVA/GA/AC composites with AC3 and AC4.

by significant contribution of nanopores in contrast to the PSD of the first series samples (Figure 1). Comparing all the results, one can assume that the main reason for low textural characteristics of the first series of composites (Table 1) was great content of GA blocking the AC nanopores.

The effects of the PVA/GA and PVA/GA/AC compositions appear in interaction with myoglobin under static (equilibrium) and dynamic (flow, diffusion) conditions described in detail in the Supporting Information (Figures S3−S5), as well as in the case of adsorption of methylene blue, MB (Figure S6, Supporting Information). Thus, improved accessibility of the AC surface in the composites results in the improved adsorption capacity of the composites with respect to both low- (MB) and high-molecular (myoglobin) compounds.

CONCLUSIONS

PVA/GA/AC composites prepared in the form of monolithic rods using the cryotropic gelation technique with the addition of carbon microparticles (content ratio AC/PVA ~ 0.2) before PVA cross-linking by GA are characterized by a porosity (S_{BET} < 100 m^2/g, V_p ~ 0.2 cm^3/g) that is close to that of GA/PVA cryogels due to the blocking of pores in AC particles by the polymer that subsequently undergoes cross-linking. An increase in the AC content in composites (up to content ratio AC/PVA ~ 2), prepared as a mechanical PVA/GA and AC mixture with subsequent attachment of ACs to the PVA macropore walls by the cross-linker, leads to an increase in the contribution of

nanopores, which become more accessible. Apparently the flexibility of mobile PVA tails and trains and the availability of GA oligomers result in a strong blocking of AC pores due to the reactions of PVA/AC with GA. However, both the porosity and specific surface area of PVA/GA/AC samples increase with increasing AC content. Much higher values of these textural characteristics (S_{BET} ~ 500 m^2/g and V_p ~ 0.6 cm^3/g) are observed in the composites formed with a lower concentration of the cross-linker GA (content ratio PVA/GA/AC ~ 5/0.5/3). Thus, the negative effect of GA on the accessibility of the AC surfaces is much stronger than the PVA effect because smaller GA molecules can more easily penetrate into nanopores and narrow mesopores of AC microparticles than larger PVA macromolecules. The inner porosity of the PVA/GA walls of macropores is relatively low (V_p < 0.3 cm^3/g and S_{BET} < 100 m^2/g) because of the high pressure of ice crystallites onto the soft walls during cryotropic gelation.

Quantum-chemical calculations show that despite the fact that the values of energy of each of the hydrogen bonds between PVA or water molecules with O-containing functionalities of AC are similar polymer can displace water molecules from the carbon particle surfaces. This is in contrast to water, which cannot displace polymer from the AC surface, especially from narrow pores. This results in the formation of a tight PVA/GA shell covering the AC microparticles.

Thus, the most effective PVA/GA/AC composites for adsorption of low- and high-molecular compounds can represent a macroporous PVA/GA cryogel with loose PVA brushes (located in macropores) with bound AC microparticles without filling of their pores by PVA and especially GA. One can assume that similar regularities could be observed for cross-linked linear polymers, proteins, or starch cryogels filled by AC or other microparticles depending on the amounts of fillers and a low-molecular cross-linker.

■ ASSOCIATED CONTENT

Supporting Information

Additional figures and tables with results of quantum chemical calculations. This material is available free of charge via the Internet at http://pubs.acs.org/.

■ AUTHOR INFORMATION

Corresponding Author

*E-mail: vlad_gunko@ukr.net. Tel.: +38044-4229627. Fax: +38044-4243567.

Notes

The authors declare no competing financial interest.

■ ACKNOWLEDGMENTS

This work has been supported by the European Commission, Seventh Framework Programme, projects COMPOSITUM (PEOPLE-IRSES, grant no. 230790) and MONACO-EXTRA (PEOPLE-IAPP, grant no. 218242).

■ REFERENCES

(1) Mikhalovsky, S. V. In *Microspheres, Microcapsules and Liposomes*; Arshady, R., Ed.; Citus Books: London, 1999; Vol. 2, p 133.
(2) Tennison, S. R. *Appl. Catal., A* **1998**, *173*, 289.
(3) Tennison, S. R.; Kozynchenko, O. P.; Strelko, V. V.; Blackburn, A. J. US Patent 2004024074A1 (publ. 05 Feb 2004).
(4) Wratten, M. L. *Eur. J. Anaesth.* **2008**, *25*, 1.
(5) Howell, C. A.; Sandeman, S. R.; Phillips, G. J.; Lloyd, A. W.; Davies, J. G.; Mikhalovsky, S. V.; Tennison, S. R.; Rawlinson, A. P.; Kozynchenko, O. P.; Owen, H. L. H.; Gaylor, J. D. S.; Rouse, J. J.; Courtney, J. M. *Biomaterials* **2006**, *27*, 5286.
(6) Sandeman, S. R.; Howell, C. A.; Mikhalovsky, S. V.; Phillips, G. J.; Lloyd, A. W.; Davies, J. G.; Tennison, S. R.; Rawlinson, A. P.; Kozynchenko, O. P. *Biomaterials* **2008**, *29*, 1638.
(7) Sandeman, S. R.; Jeffery, H.; Howell, C. A.; Smith, M.; Mikhalovsky, S. V.; Lloyd, A. W. *Biomaterials* **2009**, *30*, 3143.
(8) Lozinsky, V. I. *Russ. Chem. Rev.* **2002**, *71*, 489.
(9) Plieva, F. M.; Karlsson, M.; Aguilar, M.; Gomez, D.; Mikhalovsky, S.; Galaev, I. Yu.; Mattiasson, B. *J. Appl. Polym. Sci.* **2006**, *100*, 1057.
(10) Lozinsky, V. I.; Plieva, F. M. *Enzyme Microb. Technol.* **1998**, *23*, 227.
(11) Plieva, F. M.; Galaev, I.Yu.; Noppe, W.; Mattiasson, B. *Trends Microbiol.* **2008**, *16*, 543.
(12) Ku, D. N.; Braddon; L. G.; Wootton, D. M. US patent no. 5981826, 1999.
(13) Pazos, V.; Mongrain, R.; Tardif, J. C. *J. Mech. Behav. Biomed. Mater.* **2009**, *2*, 542.
(14) Hajizadeh, S.; Kirsebom, H.; Mattiasson, B. *Soft Matter* **2010**, *6*, 5562.
(15) Harris, P. J. F. *Int. Mater. Rev.* **2004**, *49*, 31.
(16) Zhang, J.; Mine, M.; Zhu, D.; Matsuo, M. *Carbon* **2009**, *47*, 1311.
(17) Spitalsky, Z.; Tasis, D.; Papagelis, K.; Galiotis, C. *Prog. Polym. Sci.* **2010**, *35*, 357.
(18) Shaffer, M. S. P.; Windle, A. H. *Adv. Mater.* **1999**, *11*, 937.
(19) Bin, Y.; Mine, M.; Koganemaru, A.; Jiang, X.; Matsuo, M. *Polymer* **2006**, *47*, 1308.
(20) Park, B.-H.; Choi, J.-H. *Electrochim. Acta* **2010**, *55*, 2888.
(21) Laget, V.; Hornick, C.; Rabu, P.; Drillon, M. *J. Mater. Chem.* **1999**, *9*, 169.
(22) Qian, X. F.; Yin, J.; Yang, Y. F.; Lu, Q. H.; Zhu, Z. K.; Lu, J. *J. Appl. Polym. Sci.* **2001**, *82*, 2744.
(23) Gupta, A. *Int. J. Nanotechnol. Appl.* **2010**, *4*, 109.
(24) Porel, S.; Singh, S.; Sree Harsha, S.; Narayana Rao, D.; Radhakrishnan, T. P. *Chem. Mater.* **2005**, *17*, 9.
(25) Peresin, M. S.; Habibi, Y.; Zoppe, J. O.; Pawlak, J. J.; Rojas, O. J. *Biomacromolecules* **2010**, *11*, 674.
(26) Liong, M.; Shao, H.; Haun, J. B.; Lee, H.; Weissleder, R. *Adv. Mater.* **2010**, *22*, 5168.
(27) Bansal, R. C.; Donnet, J. B.; Stoeckli, F. *Active Carbon*; Marcel Dekker: New York, 1988.
(28) Schiffman, J. D.; Elimelech, M. *ACS Appl. Mater. Interfaces* **2011**, *3*, 462.
(29) Cooney, D. O. *Activated Charcoal in Medical Applications*; Marcel Dekker: New York, 1995.
(30) Marsh, H.; Rodríguez-Reinoso, F. *Activated Carbon*; Elsevier: London, 2006.
(31) Mikhalovsky, S. V.; Gun'ko, V. M.; Turov, V. V.; Leboda, R.; Betz, W. R. *Adsorption* **2005**, *11*, 657.
(32) Sandeman, S. R.; Gun'ko, V. M.; Bakalinska, O. M.; Howell, C. A.; Zheng, Y.; Kartel, M. T.; Phillips, G. J.; Mikhalovsky, S. V. *J. Colloid Interface Sci.* **2011**, *358*, 582.
(33) Gun'ko, V. M.; Turov, V. V.; Kozynchenko, O. P.; Nikolaev, V. G.; Tennison, S. R.; Meikle, S. T.; Snezhkova, E. A.; Sidorenko, A. S.; Ehrburger-Dolle, F.; Morfin, I.; Klymchuk, D. O.; Mikhalovsky, S. V. *Adsorption* **2011**, *17*, 453.
(34) Gun'ko, V. M.; Kozynchenko, O. P.; Turov, V. V.; Tennison, S. R.; Zarko, V. I.; Nychiporuk, Y. M.; Kulik, T. V.; Palyanytsya, B. B.; Osovskii, V. D.; Ptushinskii, Y. G.; Turov, V. A. *Colloids Surf. A* **2008**, *317*, 377.
(35) Gun'ko, V. M.; Turov, V. V.; Kozynchenko, O. P.; Palijczuk, D.; Szmigielski, R.; Kerus, S. V.; Gorbik, P. P. *Appl. Surf. Sci.* **2008**, *254*, 3220.
(36) McGuire, M. J.; Suffet, I. H. *Treatment of Water by Granular Activated Carbon; Advances in Chemistry Series*, N 202; Oxford University Press: Oxford, 1983.
(37) Brennan, J. K.; Bandosz, T. J.; Thomson, K. T.; Gubbins, K. E. *Colloids Surf. A* **2001**, *187–188*, 539.

(38) Peppas, N. A.; Bures, P.; Leobandung, W.; Ichikawa, H. *Eur. J. Pharm. Biopharm.* **2000**, *50*, 27.
(39) Gomes, M. E.; Holtorf, H. L.; Reis, R. L.; Mikos, A. G. *Tissue Eng.* **2006**, *12*, 801.
(40) Hwang, Y.-J.; Granelli, J.; Lyubovitsky, J. *ACS Appl. Mater. Interfaces* **2012**, *4*, 261.
(41) Bansal, V.; Roychoudhury, P. K.; Mattiasson, B.; Kumar, A. *J. Mol. Recognit.* **2006**, *19*, 332.
(42) Zhang, W.; Zhang, Z.; Wang, X. *J. Colloid Interface Sci.* **2009**, *333*, 346.
(43) Sridhar, V.; Oh, I.-K. *J. Colloid Interface Sci.* **2010**, *348*, 384.
(44) Sayed, F. N.; Grover, V.; Dubey, K. A.; Sudarsan, V.; Tyagi, A. K. *J. Colloid Interface Sci.* **2011**, *353*, 445.
(45) Bryaskova, R.; Pencheva, D.; Kale, G. M.; Lad, U.; Kantardjiev, T. *J. Colloid Interface Sci.* **2010**, *349*, 77.
(46) Kundu, S.; Huitink, D.; Wang, K.; Liang, H. *J. Colloid Interface Sci.* **2010**, *344*, 334.
(47) Gohil, J. M.; Ray, P. *J. Colloid Interface Sci.* **2009**, *338*, 121.
(48) Mattiasson, B.; Kumar, A.; Galaev, I. Yu., Eds. Macroporous Polymers. *Production, Properties and Biotechnological/Biomedical Applications*; CRC Press: Boca Raton, FL, 2009.
(49) Cui, Zh., Ed.; *Medical Biothechnology and Health Care*, Second ed.; Elsevier: New York, 2011; Vol. 5.
(50) Gun'ko, V. M.; Savina, I. N.; Mikhalovsky, S. V. *Adv. Colloid Interface Sci.* submitted for publication.
(51) Tashima, T.; Imai, M.; Kuroda, Y.; Yagi, S.; Nakagawa, T. *J. Org. Chem.* **1991**, *56*, 694.
(52) Kim, K.-J.; Lee, S.-B.; Han, N.-W. *Korean J. Chem. Eng.* **1994**, *11*, 41.
(53) Gun'ko, V. M.; Meikle, S. T.; Kozynchenko, O. P.; Tennison, S. R.; Ehrburger-Dolle, F.; Morfin, I.; Mikhalovsky, S. V. *J. Phys. Chem. C* **2011**, *115*, 10727.
(54) Neimark, A. V.; Ravikovitch, P. I. *Microporous Mesoporous Mater.* **2001**, *44/45*, 697.
(55) Nguyen, C.; Do, D. D. *Langmuir* **1999**, *15*, 3608.
(56) Gun'ko, V. M.; Do, D. D. *Colloids Surf. A* **2001**, *193*, 71.
(57) Gun'ko, V. M.; Turov, V. V. *Nuclear Magnetic Resonance Studies of Interfacial Phenomena*; Taylor & Francis: Boca Raton, 2013, in press.
(58) Gun'ko, V. M.; Mikhalovsky, S. V. *Carbon* **2004**, *42*, 843.
(59) Frisch, M. J.; Trucks, G. W.; Schlegel, H. B.; Scuseria, G. E.; Robb, M. A.; Cheeseman, J. R.; Montgomery, J. A., Jr.; Vreven, T.; Kudin, K. N.; Burant, J. C.; Millam, J. M.; Iyengar, S. S.; Tomasi, J.; Barone, V.; Mennucci, B.; Cossi, M.; Scalmani, G.; Rega, N.; Petersson, G. A.; Nakatsuji, H.; Hada, M.; Ehara, M.; Toyota, K.; Fukuda, R.; Hasegawa, J.; Ishida, M.; Nakajima, T.; Honda, Y.; Kitao, O.; Nakai, H.; Klene, M.; Li, X.; Knox, J. E.; Hratchian, H. P.; Cross, J. B.; Adamo, C.; Jaramillo, J.; Gomperts, R.; Stratmann, R. E.; Yazyev, O.; Austin, A. J.; Cammi, R.; Pomelli, C.; Ochterski, J. W.; Ayala, P. Y.; Morokuma, K.; Voth, G. A.; Salvador, P.; Dannenberg, J. J.; Zakrzewski, V. G.; Dapprich, S.; Daniels, A. D.; Strain, M. C.; Farkas, O.; Malick, D. K.; Rabuck, A. D.; Raghavachari, K.; Foresman, J. B.; Ortiz, J. V.; Cui, Q.; Baboul, A. G.; Clifford, S.; Cioslowski, J.; Stefanov, B. B.; Liu, G.; Liashenko, A.; Piskorz, P.; Komaromi, I.; Martin, R. L.; Fox, D. J.; Keith, T.; Al-Laham, M. A.; Peng, C. Y.; Nanayakkara, A.; Challacombe, M.; Gill, P. M. W.; Johnson, B.; Chen, W.; Wong, M. W.; Gonzalez, C.; Pople, J. A. *Gaussian 03*, revision E.01; Gaussian, Inc.: Wallingford, CT, 2004.
(60) Schmidt, M. W.; Baldridge, K. K.; Boatz, J. A.; Elbert, S. T.; Gordon, M. S.; Jensen, J. J.; Koseki, S.; Matsunaga, N.; Nguyen, K. A.; Su, S.; Windus, T. L.; Dupuis, M.; Montgomery, J. A. *J. Comput. Chem.* **1993**, *14*, 1347.
(61) Granovsky, A. A. http://classic.chem.msu.su/gran/gamess/index.html (Accessed Dec 4, 2009).
(62) Stewart, J. J. P. *MOPAC 2009 and 2012*; Stewart Computational Chemistry, Colorado Springs, CO, USA, 2012. http://openmopac.net/.
(63) Pedretti, A. L.; Villa, G.; Vistoli, G. *J. Comput.-Aided Mol. Design* **2004**, *18*, 167.
(64) Phillips, J. C.; Braun, R.; Wang, W.; Gumbart, J.; Tajkhorshid, E.; Villa, E.; Chipot, Ch.; Skeel, R. D.; Kale, L.; Schulten, K. *J. Comput. Chem.* **2005**, *26*, 1781. http://www.ks.uiuc.edu/Research/namd/.
(65) *Jmol*, an open-source Java viewer for chemical structures in 3D, http://jmol.sourceforge.net/.
(66) Zhurko, G. A.; Zhurko, D. A. *Chemcraft* (version 1.6, build 342), http://www.chemcraftprog.com.
(67) (a) http://rsbweb.nih.gov/ij/download.html (accessed July 2007). (b) Prodanov, D., http://rsb.info.nih.gov/ij/plugins/granulometry.html (accessed August 2007).
(68) Liu, J.-C.; Monson, P. A. *Adsorption* **2005**, *11*, 5.
(69) Palmer, J. C.; Brennan, J. K.; Hurley, M. M.; Balboa, A.; Gubbins, K. E. *Carbon* **2009**, *47*, 2904.
(70) Nguyen, T. X.; Cohaut, N.; Bae, J.-S.; Bhatia, S. K. *Langmuir* **2008**, *24*, 7912.
(71) Gun'ko, V. M.; Kozynchenko, O. P.; Tennison, S. R.; Leboda, R.; Skubiszewska-Zięba, J.; Mikhalovsky, S. V. *Carbon* **2012**, *50*, 3146.
(72) Shapiro, Yu. E. *J. Colloid Interface Sci.* **1999**, *212*, 453.